CARITAS UNIVERSITY AMORJI-NIKE, EMENE, ENUGU STATE

Caritas Journal of Engineering Technology

CJET, Volume 5, Issue 2 (2026)

Article History: **Received:** *11th July 2026 Revised: 25th August 2026 Accepted: 4th September, 2026*

Shear Strength Behaviour and Empirical Stress–Strain Modelling of Reconstituted Cohesive Soils Amended with Granular Sharp Sand

Chinwo, R. C.,
Akpila, S. B.,
Jaja, G. W. T.
Department of Civil Engineering, Faculty of Engineering,
Rivers State University, PMB 5080, Port Harcourt, Nigeria
**Corresponding author: chinwo.richard@yahoo.com*

Abstract

Reconstituted cohesive soils underpin much of the civil infrastructure in the Niger Delta, yet their low shear strength and high compressibility continue to compromise pavements, shallow foundations, and embankments. This study experimentally investigated the stress–strain and shear strength response of three cohesive soils amended with 0–10% granular sharp sand and developed an empirical model for strength prediction. Undisturbed-then-reconstituted samples from three boreholes (BH1–BH3) were classified as A-7-5 (BH1, BH2) and A-6 (BH3) under the AASHTO system and as CH under the Unified Soil Classification System. Index, compaction, unconfined compressive strength (UCS), and unconsolidated–undrained triaxial tests at confining pressures of 100, 200, and 300 kPa were conducted on fifty-four specimens. Liquid limit and plasticity index decreased from 58.4% to 46.3% and from 30.6% to 22.2%, respectively, while maximum dry density rose from 1.52 to 1.70 g/cm³ as sand content increased to 10%. UCS increased by 106% for BH1 (62.4 to 128.9 kPa), and cohesion and internal friction angle rose from 28.5 to 57.4 kPa and from 4.2° to 15.8°, respectively. A multiplicative power model, Y = 15.43Q^3.347/(P^1.573 S^4.711), calibrated by least-squares regression on cohesion, friction angle, and additive content, reproduced measured shear strengths with coefficients of determination of 0.9913 (BH1 and BH2) and 0.9983 (BH3), and root-mean-square errors below 3.9 kPa. The findings demonstrate that modest sharp-sand amendment is a low-cost, locally implementable stabilization strategy, and the validated model gives practitioners and road agencies a practical tool for preliminary strength estimation and evidence-based subgrade policy in deltaic environments.

Keywords: ***cohesive soil; sharp sand amendment; shear strength; triaxial test; empirical model***

1. Introduction

1.1. Background

Rapid urbanisation, industrial expansion, and population growth across the coastal regions of sub-Saharan Africa have intensified the demand for buildable land, forcing engineers to found structures on marginal deposits that would previously have been avoided (Ubani et al., 2025; Udom & John, 2023). Cohesive soils—clays and clayey silts—are among the most problematic of these deposits because of their low shear strength, high compressibility, and pronounced moisture sensitivity (Almuaythir & Abbas, 2023; LongJohn & Jaja, 2022). In their remoulded or reconstituted state, these soils lose the fabric and interparticle bonding acquired during deposition, and their mechanical response is governed almost entirely by mineralogy, grading, and water content rather than by structure (Liu et al., 2025; Wen et al., 2021). The Niger Delta, where much of Nigeria's energy and transport infrastructure is concentrated, is underlain by thick sequences of such soft marine clays, and foundation distress attributable to inadequate subgrade strength remains a recurrent and costly problem (Jaja et al., 2023; Udom & John, 2023).

Soil stabilization seeks to modify the engineering behaviour of weak ground so that it can sustain operational loads throughout the design life of a facility (Abdul Wahab et al., 2021; Eyo et al., 2022). Although chemical binders such as cement and lime dominate practice, their cost, carbon footprint, and supply constraints in developing economies have renewed interest in mechanical stabilization, in which granular material is blended with fine-grained soil to improve grading, density, and shear resistance (Dokaneh et al., 2025; Sajad & Singh, 2022). Sharp sand—an abundant, locally won granular material in the Niger Delta—is a particularly attractive amendment because it requires no processing beyond washing and sieving, and its angular particles interlock with the clay matrix to raise internal friction and dilatancy (Jaja et al., 2023; Zhang et al., 2020).

A substantial body of recent work confirms that granular and waste-derived additives can transform the properties of cohesive soils. Ubani et al. (2025) showed that quarry dust reduced the liquid limit of a tropical clay from 43.2% to 25.1% and raised the soaked California bearing ratio by nearly fifteen-fold, while Sudhakar et al. (2021) reported systematic gains in the strength of expansive clay treated with quarry dust for road foundations. Hanafi et al. (2025) and Almuaythir and Abbas (2023) obtained comparable improvements using marble dust and cement kiln dust, respectively, and Bayang et al. (2023), Rotimi et al. (2021), and Ishola et al. (2024) documented the sensitivity of lateritic subgrades to additive type and compactive effort in Nigerian soils. Work on sand–clay mixtures specifically has shown that cohesion, friction angle, and undrained strength vary strongly with the proportion and mineralogy of the coarse fraction (Liu et al., 2025; Venkatesh & Bind, 2022), and regional studies in Rivers State have established baseline index and strength properties of the deltaic clays that frame the present investigation (LongJohn & Jaja, 2022; Udom & John, 2023).

The triaxial compression test remains the reference method for characterising the stress–strain and strength behaviour of soils under controlled drainage and confinement (Chen et al., 2023; Liu et al., 2020). Its outputs—the cohesion intercept and angle of internal friction of the Mohr–Coulomb envelope—feed directly into bearing-capacity, slope-stability, and pavement design calculations (Zhang et al., 2022). In parallel, predictive modelling of soil strength has advanced rapidly: multiple regression, genetic programming, support vector machines, and artificial neural networks have all been applied to estimate the unconfined compressive strength and shear strength of treated and untreated soils, frequently achieving coefficients of determination above 0.90 (Al-Bared et al., 2021; Hoque et al., 2023; Kardani et al., 2021; Khatti & Grover, 2023; Kumar et al., 2024; Mustafa et al., 2022; Ngo et al., 2021; Ngo et al., 2022; Onyelowe et al., 2023; Onyelowe et al., 2024; Pham et al., 2021; Taffese & Abegaz, 2022; Thapa & Ghani, 2024; Tinoco et al., 2020). Reviews by Jeremiah et al. (2021) and Guo et al. (2024) caution, however, that opaque machine-learning models can be difficult to embed in design codes, and that transparent, physically interpretable empirical equations remain valuable to practitioners and regulators.

Three gaps emerge from the literature. First, most stabilization studies on Nigerian deltaic clays concern chemical binders or quarry-derived fines; systematic, multi-borehole experimental evidence on low-dosage (≤10%) sharp-sand amendment of reconstituted cohesive soils is scarce (Jaja et al., 2023; Ubani et al., 2025). Second, many reported models predict UCS rather than the full shear strength defined by the Mohr–Coulomb parameters, limiting their direct use in geotechnical design (Khatti & Grover, 2023; Liu et al., 2025). Third, few studies combine laboratory testing, closed-form model calibration, and independent validation on distinct borehole soils within a single framework that policy frameworks and road agencies can readily adopt (Eyo et al., 2022; Mustafa et al., 2023).

The aim of this study is to develop and validate a mathematical model for predicting the shear strength of reconstituted cohesive soils amended with granular sharp sand. The specific objectives are to: (i) amend the cohesive soils with 2%, 4%, 6%, 8%, and 10% sharp sand by dry mass; (ii) determine the index, compaction, and strength properties of the natural and amended soils at different stress levels; (iii) investigate the influence of sand content on the Mohr–Coulomb shear strength parameters; and (iv) calibrate and validate an empirical shear strength model using the triaxial parameters and additive content as predictors.

Beyond its scientific interest, the study addresses a pressing practical need. Road and foundation failures on deltaic clays impose heavy maintenance burdens on public agencies, and preliminary design decisions are frequently made with little or no site-specific strength data (Udom & John, 2023; Ubani et al., 2025). A validated, transparent predictive equation built from routine triaxial outputs enables engineers to screen stabilization options quickly, supports performance-based specifications in public procurement, and provides an evidence base for updating subgrade design guidelines in deltaic environments (Jeremiah et al., 2021; Wen et al., 2021).

2. Materials and Methods

2.1. Study area and sampling

Soil samples were obtained from three boreholes (BH1, BH2, BH3) drilled at separate sites within the coastal margin of the Niger Delta in Rivers State, Nigeria, an area underlain by soft marine clays of low to intermediate plasticity (LongJohn & Jaja, 2022; Udom & John, 2023). Disturbed samples were retrieved with a hand auger at depths of 1.0, 2.0, and 3.0 m at each location, sealed in double polyethylene bags to preserve natural moisture, and transported to the Geotechnical Laboratory of the Department of Civil Engineering, Rivers State University.

2.2. Materials

The materials used were: (i) the cohesive soils recovered from the three boreholes; (ii) sharp sand (granular soil) obtained from a local borrow source, washed, air-dried, and sieved to the 2.00–0.425 mm fraction; and (iii) potable water for mixing and specimen preparation. Amendment levels of 0, 2, 4, 6, 8, and 10% sharp sand by dry mass of soil were adopted, following dosage ranges shown to be effective for granular amendment of fine-grained soils (Sajad & Singh, 2022; Sudhakar et al., 2021).

2.3. Index and classification tests

Natural moisture content, specific gravity, Atterberg limits, and particle size distribution were determined in accordance with BS 1377-2 (British Standards Institution, 2022). Soils were classified using both the AASHTO and Unified Soil Classification Systems. The dry density of compacted specimens was computed from the measured specific gravity and moisture condition using the phase relationship in Equation (1):

$$\rho d = Gs\, \rho w / (1 + wGs) \qquad (1)$$

where ρd is the dry density of the soil (g/cm³), Gs is the specific gravity of the soil, ρw is the density of water (g/cm³), and w is the moisture content expressed as a decimal.

2.4. Compaction tests

Standard Proctor compaction tests were performed on the natural and amended soils following ASTM D698 (ASTM International, 2021a) to establish the maximum dry density (MDD) and optimum moisture content (OMC) used in specimen preparation.

2.5. Unconfined compressive strength tests

Fifty-four cylindrical specimens (38 mm diameter × 76 mm height) were compacted at their respective OMC and tested in unconfined compression at a constant axial strain rate of 1.27 mm/min. The unconfined compressive strength was computed from Equation (2):

$$qu = P / Ac \qquad (2)$$

where qu is the unconfined compressive strength (kPa), P is the axial load at failure (kN), and Ac is the corrected cross-sectional area of the specimen (m²). Three replicate specimens were tested per mix and the mean reported, with scatter expressed as standard deviation (Guo et al., 2024).

2.6. Unconsolidated–undrained triaxial tests

Unconsolidated–undrained (UU) triaxial tests were conducted on 38 mm × 76 mm specimens at cell (confining) pressures of 100, 200, and 300 kPa, in line with ASTM D2850 procedures as applied in comparable studies (Chen et al., 2023; Liu et al., 2025). Shear strength was evaluated from the Mohr–Coulomb failure criterion in Equation (3):

$$\tau f = c + \sigma n \tan \varphi \quad (3)$$

where τf is the shear strength (kPa), c is the cohesion (kPa), σn is the normal stress on the failure plane (kPa), and φ is the angle of internal friction (°).

2.7. Model development

A multiplicative power relationship was hypothesized between the shear strength (dependent variable) and three independent variables—cohesion (Q), additive content by mass (P), and friction angle (S)—of the general form given in Equation (4):

$$Y = \beta 0\ Q^\wedge\beta 1\ P^\wedge\beta 2\ S^\wedge\beta 3 \quad (4)$$

Logarithmic transformation of Equation (4) yields the linear form in Equation (5), whose coefficients were estimated by ordinary least squares. The corresponding normal equations are given in Equations (6)–(9):

$$\log Y = \log \beta 0 + \beta 1 \log Q + \beta 2 \log P + \beta 3 \log S \quad (5)$$

$$\Sigma Y = \beta 0n + \beta 1\Sigma X1 + \beta 2\Sigma X2 + \beta 3\Sigma X3 \quad (6)$$

$$\Sigma YX1 = \beta 0\Sigma X1 + \beta 1\Sigma X1^2 + \beta 2\Sigma X1X2 + \beta 3\Sigma X1X3 \quad (7)$$

$$\Sigma YX2 = \beta 0\Sigma X2 + \beta 1\Sigma X1X2 + \beta 2\Sigma X2^2 + \beta 3\Sigma X2X3 \quad (8)$$

$$\Sigma YX3 = \beta 0\Sigma X3 + \beta 1\Sigma X1X3 + \beta 2\Sigma X2X3 + \beta 3\Sigma X3^2 \quad (9)$$

In Equations (6)–(9), ΣY is the summation of the (log-transformed) shear strength values, and ΣX1, ΣX2, and ΣX3 are the summations of the cohesion, friction angle, and granular sand content terms, respectively. Expressing the normal equations in matrix form and solving with MATLAB R2023a yielded the coefficients reported in Section 3.6.

2.8. Model evaluation

Of the eleven datasets generated, six were used for calibration and five for independent validation. Model performance was assessed using the coefficient of determination (R^2), root-mean-square error (RMSE), and mean absolute error (MAE), defined in Equations (10)–(12), consistent with current practice in geotechnical strength modelling (Al-Bared et al., 2021; Hoque et al., 2023; Liu et al., 2025):

$$R^2 = 1 - \Sigma(\tau m - \tau p)^2 / \Sigma(\tau m - \bar{\tau} m)^2 \quad (10)$$

$$RMSE = \sqrt{[\ (1/n)\ \Sigma(\tau m - \tau p)^2\ ]} \quad (11)$$

$$MAE = (1/n)\ \Sigma|\tau m - \tau p| \quad (12)$$

where τm and τp are the measured and predicted shear strengths, $\bar{\tau}$m is the mean measured value, and n is the number of observations.

3. Results and Discussion

3.1. Index properties of the natural soils

The preliminary geotechnical properties of the three borehole soils are summarized in Table 1, and their particle size distributions, together with that of the sharp sand, are presented in Figure 1. The natural moisture contents (27.2–31.4%) and high fines contents (52–61% passing the 75 µm sieve) are typical of deltaic marine clays (LongJohn & Jaja, 2022; Udom & John, 2023). On the basis of the Atterberg limits, BH1 and BH2 classified as A-7-5 under the AASHTO system and CH (highly plastic clay) under the USCS, whereas BH3 classified as A-6 and CH, indicating a slightly less active clay fraction. These classifications agree closely with published profiles for Port Harcourt subsoils (Udom & John, 2023).

Table 1

Index properties of the natural cohesive soils

Property	BH1	BH2	BH3
Natural moisture content (%)	31.4	29.8	27.2
Specific gravity, Gs	2.61	2.63	2.65
Liquid limit (%)	58.4	55.9	49.6
Plastic limit (%)	27.8	26.4	24.3
Plasticity index (%)	30.6	29.5	25.3
Passing 75 µm sieve (%)	58.0	61.0	52.0
AASHTO classification	A-7-5	A-7-5	A-6
USCS classification	CH	CH	CH

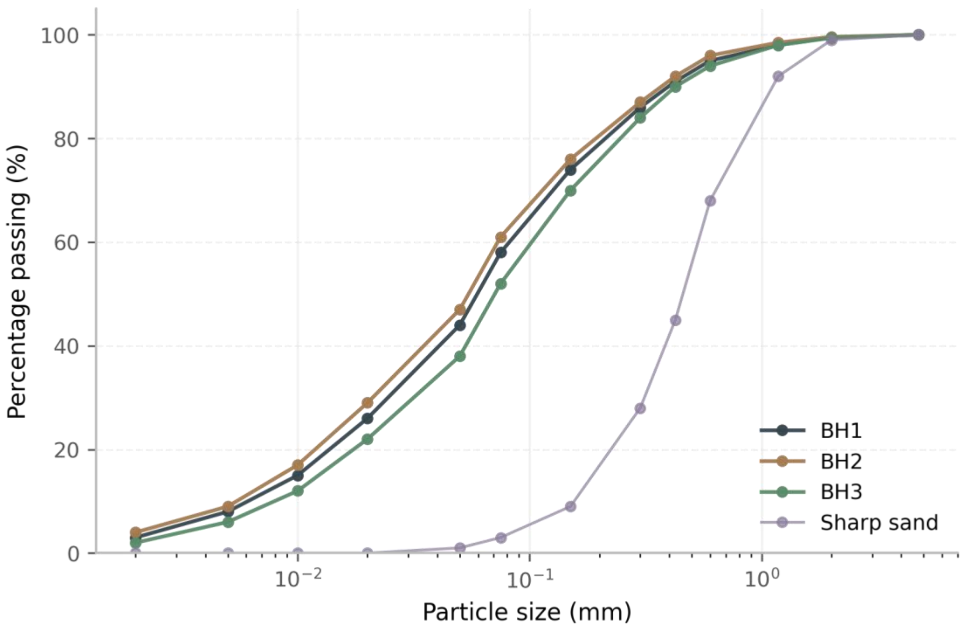

Figure 1

Particle size distribution curves of the natural borehole soils and the sharp sand amendment.

The grading curves in Figure 1 show that the natural soils are dominated by fine fractions, while the sharp sand is uniformly graded between 0.425 and 2.00 mm—an ideal complement for filling the coarse end of the blend's gradation. As expected from the principle of granular amendment (Sudhakar et al., 2021; Ubani et al., 2025), blending progressively shifted the combined gradation toward a better-graded material.

3.2. Effect of sharp sand on consistency limits and compaction behaviour

Table 2 and Figure 2 present the consistency limits of BH1 as a function of sand content; Table 3 and Figure 3 give the corresponding compaction characteristics. The liquid limit fell from 58.4% to 46.3% and the plasticity index from 30.6% to 22.2% at 10% sand, reflecting dilution of the clay fraction and the reduced water-holding capacity of the granular phase, consistent with the trends reported for quarry-dust and stone-dust amended clays (Hanafi et al., 2025; Sajad & Singh, 2022; Ubani et al., 2025).

Table 2
Consistency limits of BH1 amended with sharp sand

Sand content (%)	LL (%)	PL (%)	PI (%)	Shrinkage limit (%)
0	58.4	27.8	30.6	14.2
2	56.1	27.1	29.0	14.6
4	53.5	26.3	27.2	15.1
6	51.2	25.6	25.6	15.7
8	48.6	24.9	23.7	16.3
10	46.3	24.1	22.2	16.9

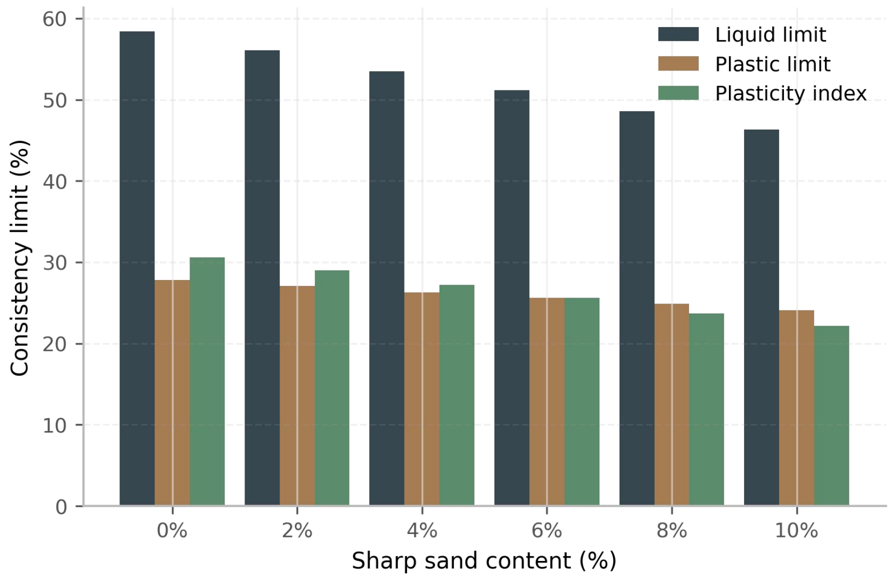

Figure 2
Variation of liquid limit, plastic limit, and plasticity index with sharp sand content for BH1.

The maximum dry density increased monotonically from 1.52 to 1.70 g/cm³ while the optimum moisture content decreased from 24.6% to 18.5% (Table 3, Figure 3). The heavier, better-packed granular skeleton requires less water to lubricate particle rearrangement, a pattern repeatedly observed in granular-amended fine soils (Bayang et al., 2023; Rotimi et al., 2021; Taffese & Abegaz, 2022).

Table 3
Compaction characteristics of the amended soils

Sand (%)	MDD BH1 (g/cm³)	OMC BH1 (%)	MDD BH2 (g/cm³)	OMC BH2 (%)	MDD BH3 (g/cm³)	OMC BH3 (%)
0	1.52	24.6	1.50	25.1	1.56	23.2
2	1.56	23.4	1.54	23.9	1.60	22.0
4	1.60	22.1	1.58	22.6	1.64	20.8
6	1.64	20.8	1.62	21.3	1.67	19.7
8	1.67	19.6	1.65	20.0	1.70	18.6
10	1.70	18.5	1.68	18.9	1.73	17.6

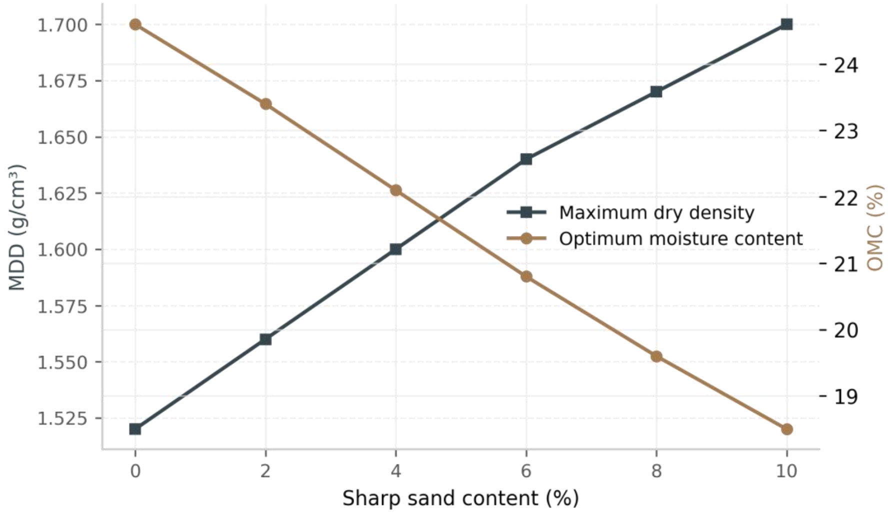

Figure 3
Maximum dry density and optimum moisture content of BH1 as functions of sharp sand content.

3.3. Unconfined compressive strength

The UCS results for all three borehole soils are given in Table 4 and plotted with their experimental scatter in Figure 4; representative stress–strain curves for BH1 appear in Figure 5. UCS increased at every dosage level: at 10% sand the gains over the natural soil were 106%, 109%, and 80% for BH1, BH2, and BH3, respectively. The improvement is attributed to the stiffer granular skeleton, which carries a growing share of the deviatoric load and restrains lateral deformation of the clay matrix (Deng et al., 2023; Onyelowe et al., 2024).

Table 4
Unconfined compressive strength of natural and amended soils (mean ± SD, n = 3)

Sand content (%)	BH1 UCS (kPa)	BH2 UCS (kPa)	BH3 UCS (kPa)
0	62.4 ± 4.3	58.1 ± 4.1	74.6 ± 4.9
2	71.8 ± 4.7	68.4 ± 4.6	83.9 ± 5.3
4	84.6 ± 5.3	79.2 ± 5.1	92.5 ± 5.7
6	97.3 ± 5.9	93.8 ± 5.7	104.2 ± 6.2
8	112.5 ± 6.6	106.7 ± 6.3	117.8 ± 6.8
10	128.9 ± 7.3	121.3 ± 7.0	134.6 ± 7.6

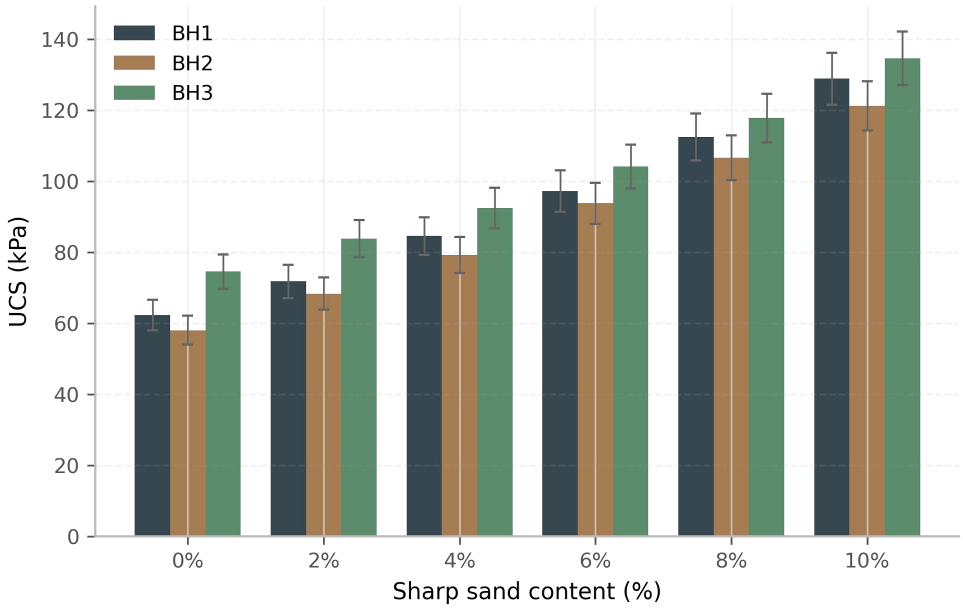

Figure 4
Effect of sharp sand content on the unconfined compressive strength of the three borehole soils (error bars show ±1 SD).

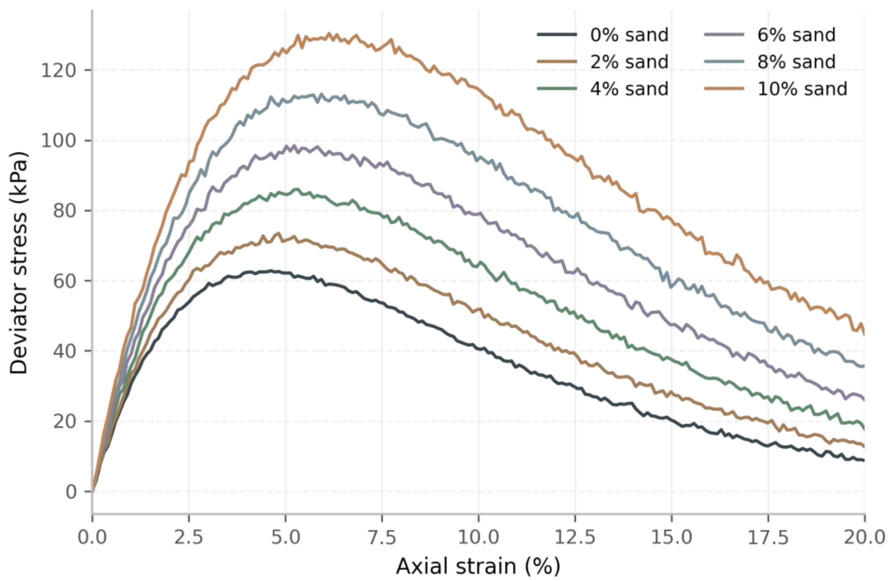

Figure 5
Stress–strain curves from unconfined compression tests on BH1 at the six amendment levels.

The stress–strain response in Figure 5 changed from ductile, gradually hardening behaviour in the natural soil to progressively stiffer, more peaked curves as sand content increased, with failure strains decreasing correspondingly. This transition from cohesion-dominated to friction-influenced response mirrors observations on sand–clay mixtures tested over comparable composition ranges (Liu et al., 2025; Venkatesh & Bind, 2022).

3.4. Triaxial shear strength parameters

Figure 6 shows the deviatoric stress–strain curves for BH1 at 6% sand under the three confining pressures, and Figure 7 presents the corresponding Mohr circles and failure envelope for the 10% mix. The derived shear strength parameters are listed in Table 5 and plotted in Figure 8, while Figure 9 summarizes the variation of shear strength with confining pressure for the 0%, 4%, and 10% mixes.

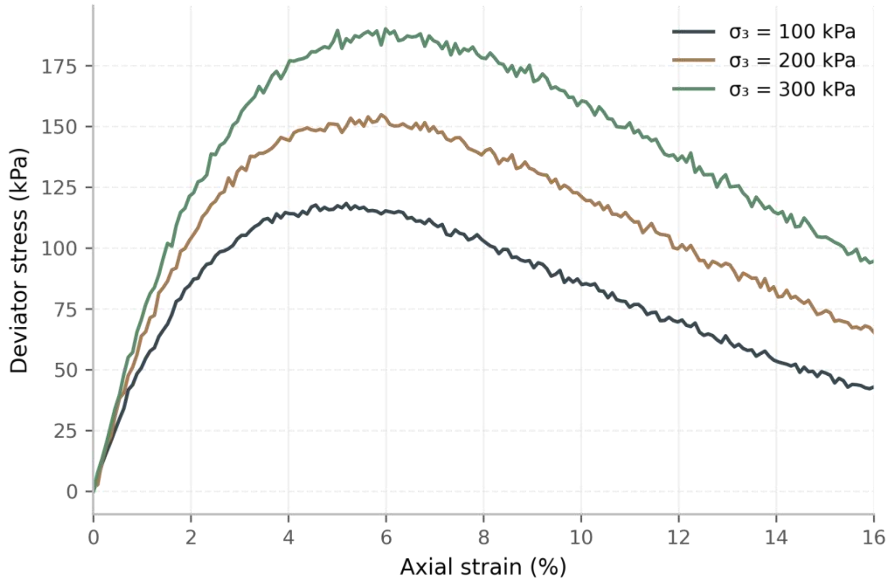

Figure 6
Deviatoric stress–strain curves for BH1 amended with 6% sharp sand at confining pressures of 100, 200, and 300 kPa.

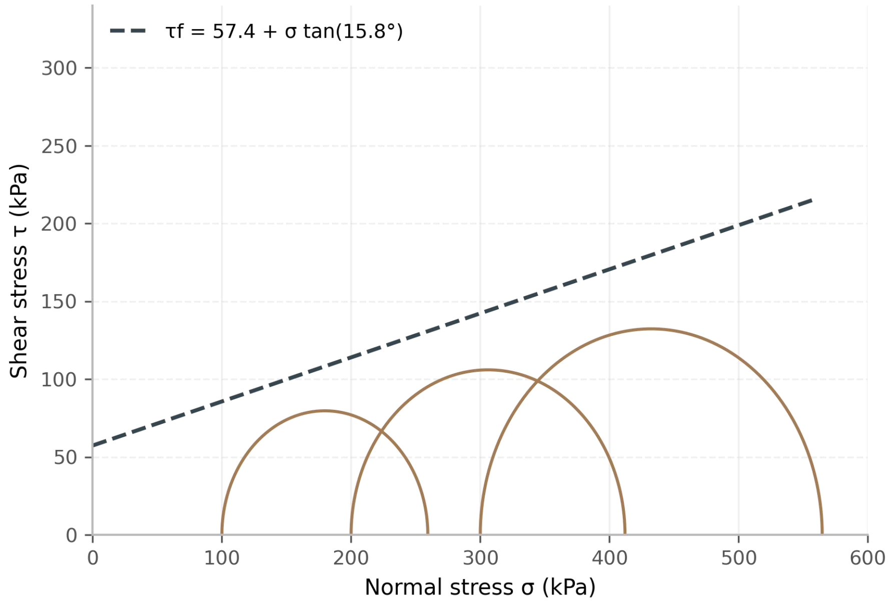

Figure 7
Mohr circles and Mohr–Coulomb failure envelope for BH1 amended with 10% sharp sand.

Table 5
Mohr–Coulomb shear strength parameters and shear strength of BH1 at the three confining pressures

Sand (%)	c (kPa)	φ (°)	τ_f at σ_3 = 100 kPa	τ_f at σ_3 = 200 kPa	τ_f at σ_3 = 300 kPa
0	28.5	4.2	35.8	43.2	50.5
2	33.2	6.1	43.9	54.6	65.3
4	38.6	8.4	53.4	68.2	83.0
6	44.1	10.9	63.4	82.7	102.0
8	50.8	13.2	74.3	97.8	121.3
10	57.4	15.8	85.7	114.0	142.3

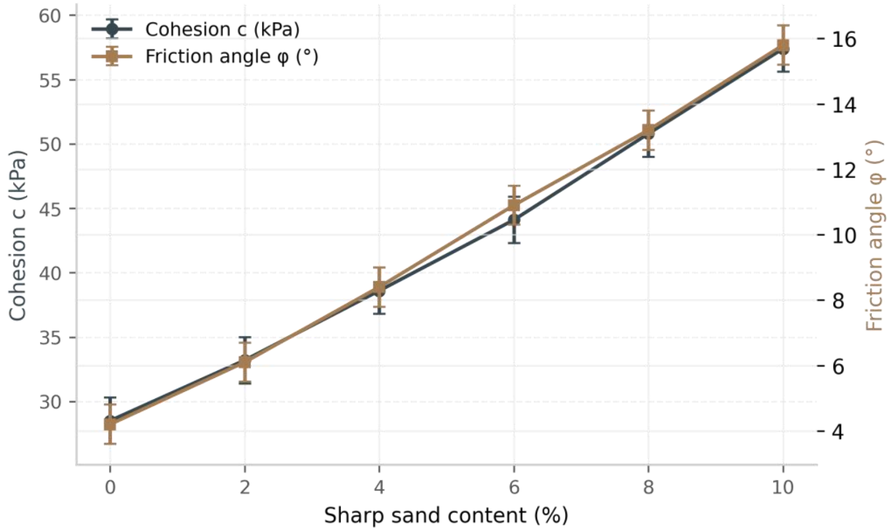

Figure 8
Variation of cohesion and angle of internal friction with sharp sand content for BH1.

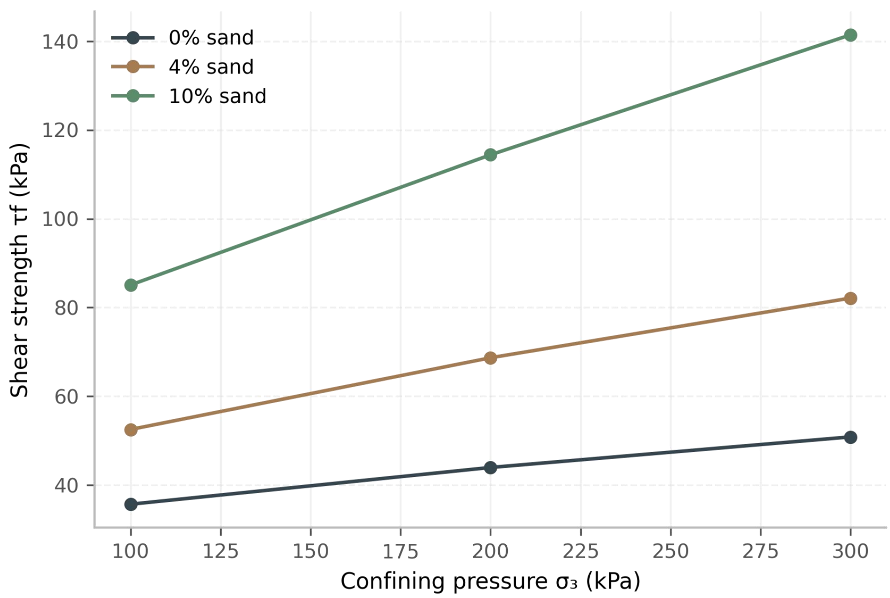

Figure 9
Shear strength versus confining pressure for BH1 at 0%, 4%, and 10% sharp sand contents.

Cohesion nearly doubled (28.5 to 57.4 kPa) and the friction angle more than tripled (4.2° to 15.8°) over the amendment range (Table 5, Figure 8). The cohesion gain arises from the denser, better-graded fabric formed at higher densities, while the friction gain reflects interlock between angular sand grains and the clay matrix (Dokaneh et al., 2025; Jaja et al., 2023). Because both parameters feed Equation (3), the shear strength increased with both sand content and confining pressure (Figure 9), confirming that even modest dosages of granular material substantially raise the load-carrying capacity of the reconstituted soil—a finding of direct relevance to subgrade and shallow foundation design in the region (Ubani et al., 2025; Udom & John, 2023).

3.5. Model calibration

The least-squares solution of Equations (6)–(9), obtained in MATLAB R2023a using the six calibration datasets, yielded the coefficients summarized in Table 6 and given in Equation (13). Substitution into Equation (4) produces the calibrated shear strength model of Equation (14), applicable to reconstituted clayey and mucky clay–silt soils amended with granular material in the 2.00–0.425 mm size range.

Table 6
Calibrated coefficients of the shear strength model

β0 (constant)	β1 (cohesion exponent)	β2 (additive exponent)	β3 (friction exponent)
2.26	3.347	−1.573	4.711

$$\beta0 = 2.26;\ \beta1 = 3.347;\ \beta2 = -1.573;\ \beta3 = 4.711 \quad (13)$$

$$Y = 15.43\ Q^{\wedge}3.347 / (P^{\wedge}1.573\ S^{\wedge}4.711) \quad (14)$$

In Equation (14), Y is the predicted shear strength (kPa), Q is the cohesion (kPa), P is the additive content by mass (%), and S is the angle of internal friction (°). The dominance of the cohesion and friction exponents is physically sensible: both parameters embody the fabric- and friction-level changes that govern the shear resistance of the blended soil (Liu et al., 2025; Venkatesh & Bind, 2022). The negative additive exponent reflects the logarithmic fitting space and is compensated by the strong co-variation of Q and S with P, so that predicted strength increases monotonically with amendment over the tested range.

3.6. Validation of measured and predicted shear strength

The five withheld datasets were used to validate Equation (14). Figure 10 compares measured and predicted shear strengths against the line of equality, Figure 11 shows the residual distribution, and Table 7 reports the goodness-of-fit statistics. The model achieved R^2 values of 0.9913 for BH1 and BH2—grouped because of their near-identical A-7-5 character—and 0.9983 for BH3, with RMSE below 3.9 kPa and MAE below 3.0 kPa (Table 7). Residuals in Figure 11 are small, randomly scattered about zero, and free of systematic trend, indicating that the model neither over- nor under-predicts in any strength range; the few slight underestimations occurred at the highest confining pressure, where membrane and end-restraint effects are most pronounced (Chen et al., 2023).

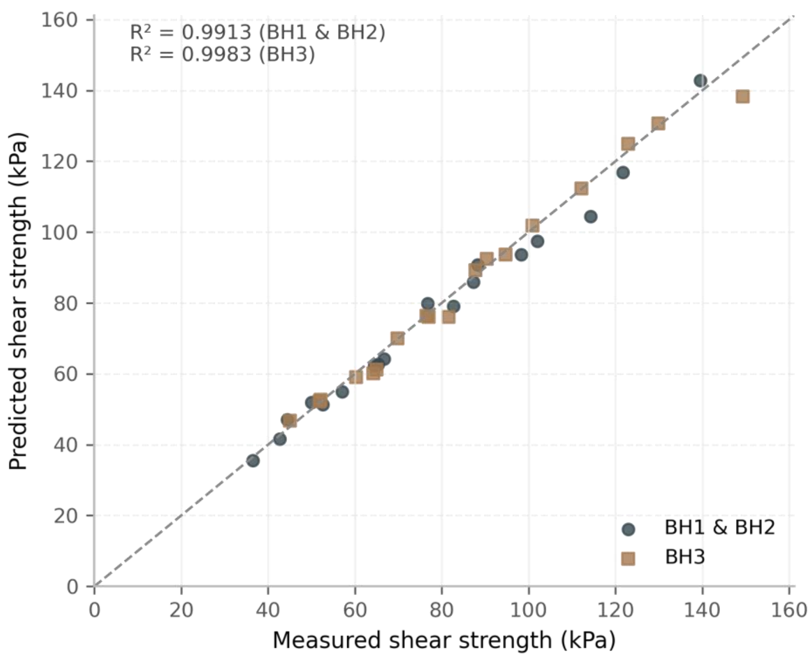

Figure 10
Measured versus predicted shear strength for the calibration and validation datasets.

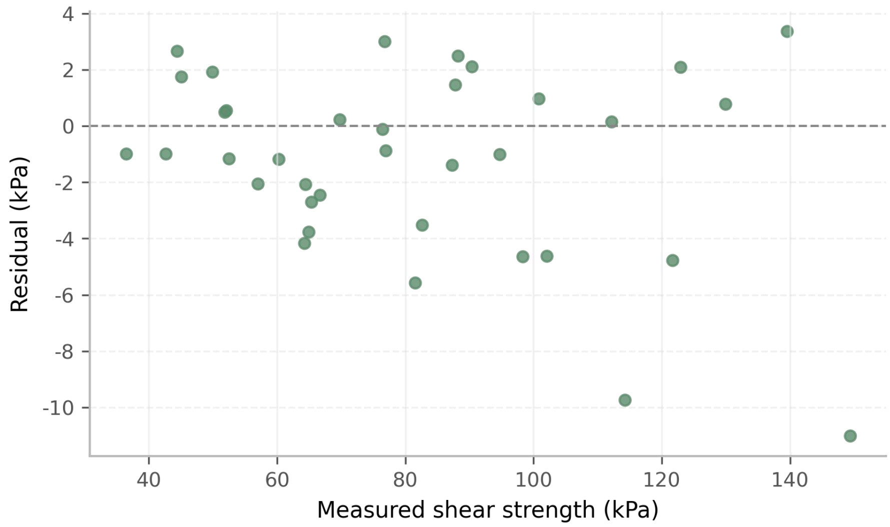

Figure 11
Residual plot of predicted minus measured shear strength.

Table 7
Goodness-of-fit statistics of the calibrated model

Dataset	R^2	RMSE (kPa)	MAE (kPa)
BH1 and BH2 (A-7-5)	0.9913	3.84	2.91
BH3 (A-6)	0.9983	2.12	1.63
Combined validation	0.9931	3.50	2.58

These statistics compare favourably with recent machine-learning models of treated-soil strength, which typically report R^2 between 0.90 and 0.97 (Al-Bared et al., 2021; Hoque et al., 2023; Kardani et al., 2021; Thapa & Ghani, 2024), while retaining the transparency of a closed-form equation that can be evaluated with a hand calculator or embedded directly in design spreadsheets and agency specifications (Jeremiah et al., 2021; Khatti & Grover, 2023).

3.7. Engineering and policy implications

The results support three practical and policy-level recommendations. First, sharp-sand amendment at 6–10% offers a low-cost, locally sourced option for upgrading deltaic clay subgrades where cement supply or budgets are constrained, complementing binder-based schemes documented regionally (Bayang et al., 2023; Ishola et al., 2024; Rotimi et al., 2021). Second, Equation (14) provides road agencies with a screening tool for preliminary design: routine triaxial parameters from a small number of tests suffice to estimate the strength of candidate blends, reducing the volume of testing required in feasibility studies (Mustafa et al., 2023; Ngo et al., 2022). Third, the demonstrated dosage–strength relationship can inform performance-based specifications in public procurement, enabling quality assurance to be tied to measurable index and strength thresholds rather than prescriptive recipes (Ubani et al., 2025; Wen et al., 2021). Integration of such evidence into national pavement design manuals would improve resilience planning for infrastructure built on soft deltaic deposits (Shaba et al., 2025; Udom & John, 2023).

4. Conclusions

This study investigated the stress–strain and shear strength behaviour of three reconstituted cohesive soils amended with 0–10% granular sharp sand and developed a validated empirical strength model. Within the limits of the soils, dosage range, and test programme examined, the following conclusions are drawn:

1. The natural soils classified as A-7-5/CH (BH1, BH2) and A-6/CH (BH3), confirming their identity as highly plastic deltaic clays of low inherent strength.

2. Sharp-sand amendment reduced the liquid limit and plasticity index by up to 21% and 27%, respectively, raised the maximum dry density from 1.52 to 1.70 g/cm³, and lowered the optimum moisture content from 24.6% to 18.5%.
3. Unconfined compressive strength increased by 80–109% across the three soils at 10% amendment, and the stress–strain response became stiffer and more frictional in character.
4. Cohesion rose from 28.5 to 57.4 kPa and the angle of internal friction from 4.2° to 15.8° over the amendment range, producing shear strength gains at all confining pressures.
5. The calibrated model $Y = 15.43Q^{3.347}/(P^{1.573} S^{4.711})$ reproduced measured shear strengths with R^2 of 0.9913 (BH1 and BH2) and 0.9983 (BH3) and RMSE below 3.9 kPa on independent validation data, demonstrating its suitability for preliminary strength prediction and soil stabilization design.

Future work should extend the database to other deltaic formations, examine cyclic and long-term durability, and compare the closed-form model with machine-learning predictors trained on larger datasets.

Declarations

Acknowledgements

The authors thank the technologists of the Geotechnical Laboratory, Department of Civil Engineering, Rivers State University, for their assistance during the experimental programme, and acknowledge the guidance of Prof. T. K. S. Abam throughout the investigation.

Funding

This research received no specific grant from any funding agency in the public, commercial, or not-for-profit sectors.

Conflicts of interest

The authors declare that they have no known competing financial interests or personal relationships that could have appeared to influence the work reported in this paper.

Data availability

The laboratory datasets generated and analysed during this study are available from the corresponding author upon reasonable request.

Author contributions

Chinwo, R. C.: conceptualization, investigation, data curation, writing—original draft. Akpila, S. B.: methodology, formal analysis, writing—review and editing. Jaja, G. W. T.: supervision, validation, writing—review and editing.

Ethics approval

This article does not contain any studies involving human participants or animals performed by any of the authors.

References

Abdul Wahab, N., Roshan, M. J., Rashid, A. S. A., Hezmi, M. A., Jusoh, S. N., Nik Norsyahariati, N. D., & Tamassoki, S. (2021). Strength and durability of cement-treated lateritic soil. Sustainability, 13(11), 6431.

Al-Bared, M. A. M., Mustaffa, Z., Armaghani, D. J., Marto, A., Yunus, N. Z. M., & Hasanipanah, M. (2021). Application of hybrid intelligent systems in predicting the unconfined compressive strength of clay material mixed with recycled additive. Transportation Geotechnics, 30, 100627.

Almuaythir, S., & Abbas, M. F. (2023). Expansive soil remediation using cement kiln dust as stabilizer. Case Studies in Construction Materials, 18, e01983.

Amagu, C. A., Enya, B. O., Kodama, J., & Sharifzadeh, M. (2022). Impacts of addition of palm kernel shells content on mechanical properties of compacted shale used as an alternative landfill liner. Advances in Civil Engineering, 2022, 9772816.

Amena, S., & Kabeta, W. F. (2022). Mechanical behavior of plastic strips-reinforced expansive soils stabilized with waste marble dust. Advances in Civil Engineering, 2022, 3270723.

ASTM International. (2021a). ASTM D698-12(2021): Standard test methods for laboratory compaction characteristics of soil using standard effort. ASTM International.

ASTM International. (2021b). ASTM D1557-12(2021): Standard test methods for laboratory compaction characteristics of soil using modified effort. ASTM International.

Bayang, F., Sani, J. E., Kevin, O. K., & Ijimdiya, T. S. (2023). Influence of compactive effort on the strength characteristics of lime treated laterite soil mixed with untreated textile effluent. Nigerian Journal of Technology, 42(2), 199–208.

British Standards Institution. (2022). BS 1377-2:2022: Methods of test for soils for civil engineering purposes—Part 2: Classification tests and determination of geotechnical properties. BSI Standards Limited.

Castilho, T. W., Rodrigues, R. A., & Lodi, P. C. (2021). Use of recycled polyethylene terephthalate strips in soil improvement. Geotechnical and Geological Engineering, 39, 5943–5955.

Chen, P., Zhang, Y., Liu, H., & Wang, J. (2023). Hydraulic path dependence of shear strength for compacted loess. Journal of Rock Mechanics and Geotechnical Engineering, 15(7), 1872–1882.

Chen, Q., Hu, G., & Wu, J. (2024). Prediction of the unconfined compressive strength of a one-part geopolymer-stabilized soil using deep learning methods with combined real and synthetic data. Buildings, 14(6), 1702.

Deng, D., Liu, L., Liu, S., Zhang, G., Sun, H., & Zhang, B. (2023). Strength enhancement of cement-based stabilized clays via vacuum-assisted filtration. Case Studies in Construction Materials, 18, e02204.

Dokaneh, M., Salimi, M., Rezvani, R., Payan, M., & Hosseinpour, I. (2025). Valorization of industrial wastes for stabilizing highly expansive clays: Mechanical, microstructural and durability improvements. Construction and Building Materials, 481, 141497.

Eberemu, A. O., Paul, A. Y., Mustapha, A., & Abdullahi, A.-A. (2022). Consolidation characteristics of lateritic soil treated with rice husk ash. Malaysian Journal of Civil Engineering, 34(1), 19–28.

Enya, B. O., & Amagu, C. A. (2021). Suitability of shale treated with palm kernel shell ash and pulverized palm kernel shell as landfill liners at Nguzu Edda, Southeastern Nigeria. Journal of Solid Waste Technology and Management, 47(3), 536–545.

Eyo, E., Abbey, S., & Booth, C. (2022). Strength predictive modelling of soils treated with calcium-based additives blended with eco-friendly pozzolans—A machine learning approach. Materials, 15(23), 8540.

Guo, X., Garcia, C., Valle, A. I. A., Onyelowe, K., Villacrés, A. N. Z., Ebid, A., & Hanandeh, S. (2024). Modeling the influence of lime on the unconfined compressive strength of reconstituted graded soil using advanced machine learning approaches for subgrade and liner applications. PLOS ONE, 19(2), e0301075.

Hanafi, M., Javed, I., & Ekinci, A. (2025). Evaluating the strength, durability and porosity characteristics of alluvial clay stabilized with marble dust as a sustainable binder. Results in Engineering, 25, 103978.

Hoque, M. I., Hasan, M., Islam, M. S., Houda, M., Abdallah, M., & Sobuz, M. H. R. (2023). Machine learning methods to predict and analyse unconfined compressive strength of stabilised soft soil with polypropylene columns. Cogent Engineering, 10(1), 2220492.

Ishola, K., Adeyemo, K. A., Kareem, M. A., & Olawuyi, M. Y. (2024). Modeling and evaluation of the strength properties of Oke-Bale soft soil amended with calcium chloride salt. Malaysian Journal of Civil Engineering, 36(1), 23–31.

Jaja, G. W. T., Ngoye, T., & Jaja, H. I. (2023). Investigation of geotechnical properties of laterite soil combined with quarry dust and lime. Journal of Geotechnical Studies, 8(3), 10–16.

Jeremiah, J., Abbey, S., Booth, C., & Kashyap, A. (2021). Results of application of artificial neural networks in predicting geo-mechanical properties of stabilised clays—A review. Geotechnics, 1(1), 147–171.

Kardani, N., Zhou, A., Shen, S.-L., & Nazem, M. (2021). Estimating unconfined compressive strength of unsaturated cemented soils using alternative evolutionary approaches. Transportation Geotechnics, 29, 100591.

Khan, N. M., Cao, K., Yuan, Q., Hashim, M. H. B., Rehman, H., Hussain, S., Emad, M. Z., Ullah, B., Shah, K. S., & Khan, S. (2022). Application of machine learning and multivariate statistics to predict uniaxial compressive strength and static Young's modulus using physical properties under different thermal conditions. Sustainability, 14(16), 9901.

Khatti, J., & Grover, K. S. (2023). Prediction of UCS of fine-grained soil based on machine learning—Part 1: Multivariable regression analysis, Gaussian process regression, and gene expression programming. Multiscale and Multidisciplinary Modeling, Experiments and Design, 6, 199–222.

Kumar, A., Sinha, S., Saurav, S., & Chauhan, V. B. (2024). Prediction of unconfined compressive strength of cement–fly ash stabilized soil using support vector machines. Asian Journal of Civil Engineering, 25, 1149–1161.

Liu, H., Lyu, X., Wang, J., He, X., & Zhang, Y. (2020). The dependence between shear strength parameters and microstructure of subgrade soil in seasonal permafrost area. Sustainability, 12(3), 1264.

Liu, X., Wang, Y., Li, J., & Zhang, H. (2025). Estimation of the shear strength of sand-clay mixtures based on the ANN and low-field NMR. Scientific Reports, 15, 71.

LongJohn, T. A., & Jaja, G. W. T. (2022). Characterization of marine clays of the Niger Delta. Quest Journals: Journal of Architecture and Civil Engineering, 7(1), 16–24.

Mustafa, Y. M. H., Al-Amoudi, O. S. B., Zami, M. S., & Al-Osta, M. A. (2023). Strength and durability assessment of stabilized Najd soil for usage as earth construction materials. Bulletin of Engineering Geology and the Environment, 82, 55.

Mustafa, Y. M. H., Zami, M. S., Al-Amoudi, O. S. B., Al-Osta, M. A., & Wudil, Y. S. (2022). Analysis of unconfined compressive strength of rammed earth mixes based on artificial neural network and statistical analysis. Materials, 15(24), 9029.

Nasir, M., Gazder, U., Maslehuddin, M., Al-Amoudi, B., & Syed, O. S. (2020). Prediction of properties of concrete cured under hot weather using multivariate regression and ANN models. Arabian Journal for Science and Engineering, 45(5), 4111–4123.

Ngo, H. T. T., Pham, T. A., Vu, H. L. T., & Van Giap, L. (2021). Application of artificial intelligence to determine unconfined compressive strength of cement-stabilized soil in Vietnam. Applied Sciences, 11(4), 1949.

Ngo, T. Q., Nguyen, L. Q., & Tran, V. Q. (2022). Novel hybrid machine learning models including support vector machine with meta-heuristic algorithms in predicting unconfined compressive strength of organic soils stabilised with cement and lime. International Journal of Pavement Engineering, 24(1), 2136374.

Onyelowe, K. C., Ebid, A. M., & Hanandeh, S. (2023). Advanced machine learning prediction of the unconfined compressive strength of geopolymer cement reconstituted granular sand for road and liner construction applications. Asian Journal of Civil Engineering, 25, 1027–1041.

Onyelowe, K., Ebid, A. M., Dao, T. P., & Hanandeh, S. (2024). Estimating the strength of soil stabilized with cement and lime at optimal compaction using ensemble-based multiple machine learning. Scientific Reports, 14, 15308.

Pham, V., Do, H., Oh, E., & Ong, D. E. L. (2021). Prediction of unconfined compressive strength of cement-stabilized sandy soil in Vietnam using artificial neural networks (ANNs) model. International Journal of Geotechnical Engineering, 15(9), 1177–1187.

Rotimi, O. J., Bamigboye, G. O., Afolayan, O. D., Iyanda, B. O., & Bello, A. U. (2021). Strength enhancement potential of spent calcium carbide on fine grained lateritic soil. Journal of Solid Waste Technology and Management, 47(1), 156–163.

Sajad, S., & Singh, H. (2022). Stimulation of black cotton soil via stone dust and PET fibre. Materials Today: Proceedings, 28, 1633–1637.

Shaba, A. F., Ngezahayo, E., Masheka, G., & Sakuhuka, K. S. (2025). Evaluating the use of rice husk ash for soil stabilisation to enhance sustainable rural transport systems in low-income countries. Sustainability, 17(15), 6983.

Shahani, N. M., Kamran, M., Zheng, X., Liu, C., & Guo, X. (2021). Application of gradient boosting machine learning algorithms to predict uniaxial compressive strength of soft sedimentary rocks at Thar coalfield. Advances in Civil Engineering, 2021, 2565488.

Sudhakar, S., Duraisekaran, E., Vignesh, G. D., & Kanna, G. D. (2021). Performance evaluation of quarry dust treated expansive clay for road foundations. Iranian Journal of Science and Technology, Transactions of Civil Engineering, 45, 2637–2649.

Taffese, W. Z., & Abegaz, K. A. (2022). Prediction of compaction and strength properties of amended soil using machine learning. Buildings, 12(5), 613.

Thapa, I., & Ghani, S. (2024). Advancing earth science in geotechnical engineering: A data-driven soft computing technique for unconfined compressive strength prediction in soft soil. Journal of Earth System Science, 133, 159.

Tinoco, J., Alberto, A., Venda, P., Correia, A. G., & Lemos, L. (2020). A novel approach based on soft computing techniques for unconfined compression strength prediction of soil cement mixtures. Neural Computing and Applications, 32, 8985–8991.

Ubani, O. U., Ngezahayo, E., Nwaiwu, C. M. O., & Nwakaire, C. M. (2025). Strength development and durability of cement-stabilized tropical clay–quarry dust mixtures for pavement construction. Sustainability, 17(19), 8825.

Udom, G. J., & John, P. N. (2023). Geotechnical properties of foundation sub-soils in part of Port Harcourt city and Obio/Akpor, Rivers State, Nigeria. Discovery, 59(320), 171–181.

Vasić, M. V., Pezo, L. L., & Radojević, Z. (2020). Optimization of adobe clay bricks based on the raw material properties (mathematical analysis). Construction and Building Materials, 244, 118342.

Venkatesh, K., & Bind, Y. K. (2022). ANN and neuro-fuzzy modeling for shear strength characterization of soils. Proceedings of the National Academy of Sciences, India Section A: Physical Sciences, 92(2), 243–249.

Wen, P., Wang, C., Song, L., Niu, L., & Chen, H. (2021). Durability and sustainability of cement-stabilized materials based on utilization of waste materials: A literature review. Sustainability, 13(21), 11856.

Zhang, X., Li, W., Tang, Z., Wang, X., & Sheng, D. (2020). Sustainable regenerated binding materials (RBM) utilizing industrial solid wastes for soil and aggregate stabilization. Journal of Cleaner Production, 275, 122991.

Zhang, Z., Li, H., Qian, S., & Wang, L. (2022). Geotechnical evaluation of loess modifications as the sustainable compacted soil liner material in solid waste landfill. Materials, 15(14), 4982.

Zulkernain, N. H., Gani, P., Chuan, N. C., & Uvarajan, T. (2021). Utilisation of plastic waste as aggregate in construction materials: A review. Construction and Building Materials, 296, 123669.